



Thermodynamic evaluation of high compressible steam flow in vapor compression systems used in desalination processes

Navid Sharifi*, Masoud Boroomand

Department of Aerospace Engineering, Amirkabir University of Technology, Hafez Ave., Tehran, Iran, Tel. +98 912 4980125; email: sharifnavid@aut.ac.ir

Received 14 June 2012; Accepted 28 January 2014

ABSTRACT

In the current study, some thermodynamic aspects of flow stream inside vapor compressors are investigated numerically and the effects of the geometry on compression process are clearly explained. A compressor provides the required energy for distillation process and the driving force for overcoming dynamic pressure losses inside the evaporators. Thermal compression process is frequently used in recent multi-effect desalination units. The basic phenomena within these devices are similar to ejectors and thus might be improved by a thoroughly CFD simulation. An experimental thermal-vapor compressor is investigated in both 2D and 3D approaches to reveal the flow characteristics inside the non-symmetric zones. Variations of some major thermodynamic properties (i.e. velocity, pressure, temperature, and density) are completely investigated within the compressor and useful graphs are produced. Afterwards, the numerical results are compared with experimental ones. Finally, it is shown that the flow deflection in the suction chamber is consequentially declined, which means the non-symmetric geometries have no considerable effect on the overall performance for industrial usages.

Keywords: Thermal desalination process; Vapor compression; CFD Simulation; Non-symmetric geometries

1. Introduction

Desalination can be achieved by a number of techniques. These may be classified into two categories: thermal (two phase) process, and membrane (single phase) process [1]. One of the most common ways to remove salt dissolved in seawater is distillation. Distillation is simply performed by heating seawater. Steam generated by evaporation of water is allowed to condense and produce fresh water.

Steam jet compressors (also called thermal-vapor compressors or TVC) are used to extract water vapor from the main vessel of evaporators [2]. This simple mechanical device uses high-pressure steam as the “motive flow” to compress another low-pressure flow called “suction flow.” TVCs are particularly used in the multi-effect desalination (MED) systems. The principal purpose of using the TVC for a MED unit is to return the useless steam accumulated in the condenser to the first stage of evaporators.

*Corresponding author.

A pilot-scale MED unit producing 50 tons per day of distillate water designed by Park et al. [3]. They could show a good agreement between experimental results and those obtained from their CFD simulations. Taking actual operation into account, some TVC-related factors, such as entrained steam position and motive steam parameters, were studied analytically, and the influences on the system performance were predicted through fundamental gas dynamics relations [4].

A reliable design methodology for thermal compressors with given operating conditions was introduced in [5,6]. This method revealed a practical relationship between characteristic parameters and nondimensional geometrical parameters, which could be used for geometry sizing.

The effects of back pressure on the flow behavior of the supersonic jet and the entraining capability of thermal compressors were presented in [7]. Different motive and discharge pressures were considered in [8] to obtain a modified thermo-compressor design. To use steam more efficiently, the performance of a MED-TVC was studied under the different steam properties injected to the thermo-compressor [9].

The effect of mixing zone geometry on the performance of thermo-compressors was numerically investigated in [10] and experimental modifications according to simulation results were applied to a real-life TVC installed in an industrial MED unit. Exergy analysis of a combined desalination unit with a thermo-compressor was performed in [11]. The first attempt to tackle two-phase flow aspects based on the wet steam theory was numerically performed by Sharifi et al. [12], and they produced more reasonable results compared with single-phase approach.

Since most of exergy losses in multi-effect distillation units with vapor compression systems occur in the thermal compressors, the rate of entropy generation was numerically investigated in [13]. This procedure was based on the second law of thermodynamics to obtain lower exergy loss and consequently higher entrainment ratio in MED-TVC units.

In this study, the flow pattern within a TVC is investigated by two different approaches (i.e. 2D axisymmetric modeling and complete three-dimensional simulation) to investigate the effects of nonsymmetric zones on the flow properties. Afterwards, the results are compared with experimental data to show the deviation of each modeling from the experiments.

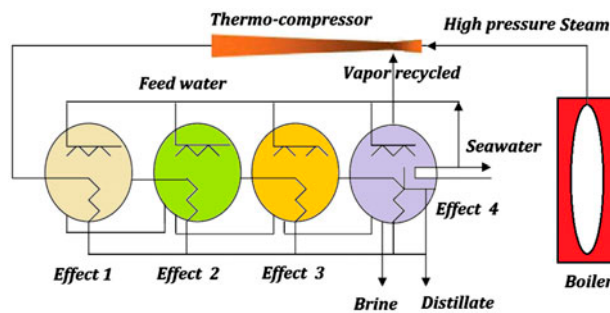


Fig. 1. Schematic of MED system with a TVC.

2. Experimental setup

2.1. Flow in a real MED system

Fig. 1 represents the flow diagram of the installation used in these tests. It shows a general MED process in which the brine water is evaporated using a heat source and the vapor is transferred to the compressor. After being pressurized in the compressor, the vapor with a higher condensation temperature returns to the first-stage evaporator where it gives its latent heat to the preheated brine. As a result, the feed inside the tubes evaporates and the vapor on the shell side gets condensed. The condensate is collected as the distillate, and the vapor produced in the last stage evaporator (i.e. condenser) goes to the compressor again for the next cycle. The experimental setup considered in this study has four stages (called effects) as shown in Fig. 2. Controls and instruments are quite similar to those found in typical industrial plants elsewhere.

The first effect is directly connected to the compressor exit. The compressed vapor is delivered completely to the shell side of the evaporator and gives its latent heat of condensation to the falling seawater film inside the tubes. Thus, some parts of the brine water inside the evaporator get evaporated and the steam from the compressor gets condensed and collected as distillate water by distillate pump.

2.2. Steam-related equipments

The required high-pressure motive steam for this MED plant is supplied from a fire tube boiler installed in the site and provides pressurized steam with a flow rate of 25 ton/h and pressure of 8 barg. It should be noted that the vacuum level inside the vessel is made up by a single-stage ejector used as a hogging ejector (i.e. startup ejector).

The presence of noncondensable gases in heat-exchanger units reduces the heat transfer efficiency



Fig. 2. Experimental setup of MED-TVC.

and increases the condensation temperature because of their low-thermal conductivity. Therefore, a smaller size ejector is used in normal operation of the system to eject the NCG gases from interior parts and prevent NCG accumulation within condensers or evaporators. This steady process removes air and noncondensable gases from the vessel at a lower flow rate compared to the rate of hogging ejector.

During the test, the primary aim is to maintain constant steam pressure and temperature on the suction side of the thermo-compressor and evaluate the maximum delivery pressure in the discharge side (i.e. 1st effect). In other words, the objective of this test is to observe variations in compression ratio over time. Because the delivery temperature is slightly higher than operating temperature of evaporators, no extra heating load is exerted on evaporators.

2.3. Seawater properties

The seawater parameter specified for regional characteristics is approximately given. Seawater temperature is 34°C, and total dissolved solid of seawater is around 41,000 ppm. Other system parameters for this experimental plant are addressed in Table 1.

Table 2 shows the measured values of pressure and flow rate at suction and discharge boundaries of the thermal compressor under different operating conditions. It is obvious from the schematic flow diagram (Fig. 1), the suction boundary is located on the last effect and the discharge boundary is connected to the first effect. These experimental values could be used to evaluate the characteristic parameters (i.e. compression ratio and entrainment ratio) which will be discussed in the last section.

3. Theory

3.1. Gas dynamics aspects

The high-pressure motive steam injected into the TVC passes through a convergent/divergent nozzle (primary nozzle) and exits at supersonic level with low-pressure in the nozzle outlet. The local pressure drop at the nozzle exit region causes a reliable suction capability to entrain the low pressure steam by employing the momentum of the supersonic flow and deliver it to the first stage of evaporators of the desalination unit.

In fact, the TVC is made up of an internal small convergent/divergent nozzle within a large one, accounted as the casing of the TVC. The convergent zone of the body in which the exiting flow from the nozzle is mixed with the suction flow and it is called as “mixing zone.” “Constant area zone” is the throat of the body in which a strong shock wave is occurred and has a great effect on the overall performance. The diverging part of the body is called “diffuser” and has an increasing effect on the pressure of subsonic flow as it goes through it.

3.2. Main characteristics

There are two important nondimensional parameters for the compression process in the thermo-compressors which are defined as below. Entrainment ratio (ω) is defined as the ratio of suction mass flow rate to motive flow rate, while compression ratio (ψ) is defined as the proportion of discharge pressure to the suction one. These values are calculated from experimental measurements for each operating condition and tabulated in Table 2.

Table 1
System parameters and experimental conditions

Experimental conditions	Value
Number of effects	4
Compression ratio	2.7–2.85
GOR	7.3–7.8
Operational pressure (mbar abs)	115–295
Total feed water flow rate in each effect (ton/h)	228–240
Feed water flow rate in each effect (ton/h)	57–60
Product water flow rate in each effect (ton/h)	18.87
Boiler pressure (barg)	8
Boiler temperature (°C)	170–180
Boiler capacity (ton/h)	25
Unit capacity (daily distillate production) (m ³ /d)	1812
Heating steam temperature in the first effect (°C)	66–69
Heating steam temperature in the second effect (°C)	62–65
Heating steam temperature in the third effect (°C)	59–61
Heating steam temperature in the fourth effect (°C)	54–58
Product quality (µs/cm)	8–11
Seawater temperature (°C)	32–38
Seawater pressure after pumping (bar)	2.5

There is a critical backpressure in which the compression effect is failed and the TVC cannot deliver the sucked steam into the low-pressure vessel (i.e. effect 1). This point of critical backpressure is normally used as a key point to calculate the exact compression ratio (ψ) of the TVC.

3.3. Operating modes

The flow behavior within a TVC falls in three distinct categories of subcritical, critical, and reversed flow modes. These different operating modes for a typical thermo-compressor are shown in Fig. 3, in which the entrainment ratio (ω) is plotted as a function of compression ratio (ψ).

As seen, entrainment ratio (ω) remains constant while the compression ratio is increased, up to the point of critical backpressure in which the normal operating mode of the TVC is decayed and entrainment ratio (ω) is rapidly dropped. The compression effect is deteriorated beyond this point and the operating mode of the compressor changed into the reverse flow mode, in which a backflow phenomenon is taken place in the suction chamber and all entered steam returns back into the vessel.

4. Numerical simulation

In order to clarify the flow behavior within a TVC, numerical simulation of steady-state compressible flow is undertaken. For this purpose, the commercial CFD code of FLUENT 6.0 was employed to simulate the complicated internal phenomena. GAMBIT 2.2 was used to create appropriate grid elements inside the calculation domain as well. In addition, all calculations were performed for both axisymmetric (2D) and full three-dimensional (3D) models of the experimental TVC.

4.1. Governing equations

The compressible flow in channels and ducts is normally governed by the general form of conservation equations of mass, momentum, and energy. The equation of state for the water vapor is used on the basis of

Table 2
Experimental results of measured data for various operating conditions

Item number	Discharge pr. (mbar)	Suction pr. (mbar)	Compression ratio	Suction flow (kg/s)	Motive flow (kg/s)	Entrainment ratio
1	279	125	2.23	5.01	6.80	0.73
2	284	124	2.29	4.76	6.57	0.72
3	303	128	2.37	5.31	7.17	0.74
4	305	123	2.48	5.51	7.58	0.73
5	311	121	2.57	5.17	7.00	0.74
6	322	120	2.68	5.32	7.14	0.75
7	333	119	2.8	4.83	6.67	0.72
8	371	128	2.9	5.16	7.44	0.69
9	381	127	3	3.63	6.84	0.53
10	381	123	3.1	1.08	7.07	0.15

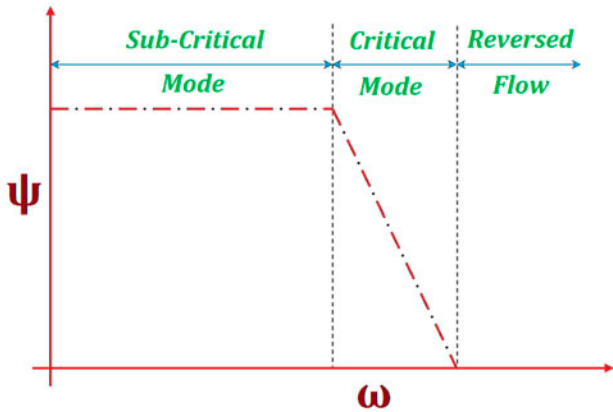


Fig. 3. Different operational modes of a typical TVC.

perfect gas law (i.e. $P = \rho RT$). Therefore, the governing equations can be written as follows:

- Mass conservation equation

$$\frac{\partial \rho}{\partial t} + \frac{\partial(\rho u_i)}{\partial x_i} = 0 \tag{1}$$

- Momentum conservation equation

$$\frac{\partial(\rho u_i)}{\partial t} + \frac{\partial}{\partial x_j}(\rho u_i u_j) = -\frac{\partial p}{\partial x_i} + \frac{\partial \tau_{ij}}{\partial x_j} \tag{2}$$

- Energy conservation equation

$$\frac{\partial(\rho E)}{\partial t} + \frac{\partial}{\partial x_i}(\rho u_i E + u_i p) = \frac{\partial p}{\partial t} + \frac{\partial}{\partial x_i} \left(k_{\text{eff}} \frac{\partial T}{\partial x_i} \right) + \frac{\partial}{\partial x_i} (u_i \tau_{ij}) \tag{3}$$

Since the mixing phenomenon of two streams is taken place in viscous conditions and affects the flow pattern strongly, it is necessary to consider an

appropriate turbulence model. The κ - ϵ turbulence and standard wall function models were selected herein. The realizable κ - ϵ model (an improved version of the conventional standard κ - ϵ model) was employed in this study. This is due to its capability for predicting more accurate spreading rate of a round jet [14].

$$\frac{\partial}{\partial t}(\rho \kappa) + \frac{\partial}{\partial x_i}(\rho \kappa u_i) = \frac{\partial}{\partial x_j} \left[(\mu + \mu_t / \sigma_\kappa) \frac{\partial \kappa}{\partial x_j} \right] + Src_\kappa \tag{4}$$

$$\frac{\partial}{\partial t}(\rho \epsilon) + \frac{\partial}{\partial x_i}(\rho \epsilon u_i) = \frac{\partial}{\partial x_j} \left[(\mu + \mu_t / \sigma_\epsilon) \frac{\partial \epsilon}{\partial x_j} \right] + Src_\epsilon \tag{5}$$

4.2. Explanation on the solver procedure

The flowchart of computational procedure that is required for solving aforementioned equations in the FLUENT software with detailed description of required inputs are presented in Appendix A.

4.3. Dimensions of computational domain

A simple layout of experimental compressor with detailed dimensions of computational domain is shown in Fig. 4. This fixed schematic layout was used to produce two different grid models.

- (1) *Grid for 2D simulation:* The number of structured elements generated for an axisymmetric model was around 28,700 quadrilateral elements as shown in Fig. 5.
- (2) *Grid for 3D simulation:* The geometry of the three-dimensional model was created similar to the axisymmetric model, and approximately, 1,485,700 structured hexahedral elements were generated to cover the entire calculation domain as shown in Fig. 6.

The main difference between these two models is pertaining to the suction side in which a non-symmetric

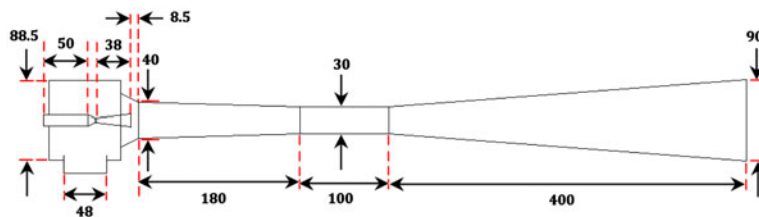


Fig. 4. Dimensions of computational domain.

zone can be observed in 3D model. This part was eliminated in 2D model due to axisymmetric solver be used, and a simpler solution method could be achieved.

4.4. Boundary conditions

In all TVC, there are two different flows entering into and one mixed flow exiting from the TVC. The “pressure inlet” type boundary condition was applied to both motive and suction flows and the “pressure outlet” type boundary condition was considered for the discharge flow. The exact values that were applied to these boundaries are listed in Table 3.

5. Results and discussion

In order to explain the flow pattern inside the TVC, it is necessary to reveal the variations of thermodynamic properties along the main axis (i.e. axis of symmetry) of the TVC. The main flow properties, which are discussed herein, are as follows: velocity, pressure, temperature, and density, because the flow field is strongly affected by variations of these fundamental parameters. It should be noted that other flow properties, such as flow Mach number, specific heat ratio, dynamic pressure and so on can be indirectly calculated based on these indicated properties.

5.1. Graphs of thermodynamic variables

Figs. 7–10 show the variations of velocity, pressure, temperature, and density along the axial direction inside the TVC for 2D (axisymmetric) and 3D approaches. As seen, approximately, similar trends for each property represent an acceptable agreement between these two numerical simulations. In other words, the 2D approach is capable of producing reasonable results as 3D one with some small discrepancies. The exact flow phenomena can be explained as follows.

The motive steam enters the TVC with a subsonic velocity ($x < 0$ on the graphs). As the stream flows in

the converging part of the nozzle, its pressure is reduced and its velocity increases ($x \approx 0$ on the graphs). The stream reaches sonic velocity at the nozzle throat, where its Mach number is equal to unity. The increase in the cross section area in the diverging part of the nozzle results in a decrease in the supersonic pressure and an increase in its velocity to higher supersonic conditions ($x > 0$ on the graphs).

At the nozzle exit plane, the motive steam pressure becomes lower than the entrained vapor pressure and its velocity ranges around 1,100 m/s. All these phenomena were illustrated in graphs in the vicinity of $x = 0$.

Afterwards, the velocity of entrained vapor entering from the suction chamber increases and its pressure decreases continuously through the sharp converging duct at the beginning of the TVC body.

The motive steam and entrained vapor streams may mix within the mixing chamber (with a smooth converging angle) or they may flow as two separate streams as they enter the constant area zone of the TVC body, where mixing process is completed. The fluctuations observed on the graphs of each property between $x \approx 0.5$ and $x \approx 2.5$ are related to the formation of oblique shock waves in the mixing zone (converging tube).

Afterwards, the mixture goes through a strong shock wave within the constant area section of the body. This phenomenon is observed around $x \approx 3.0$ on the graphs. The shock is associated with a reduction of the mixture velocity (Fig. 7), increase in the mixture pressure (Fig. 8), increase in the mixture temperature (Fig. 9), and increase in the mixture density (Fig. 10). After this position, the flow becomes subsonic and emerges from the diverging zone of the diffuser.

As mixture flow goes through the diverging zone ($x > 3.5$ on the graphs), further pressure increase and velocity decrease occur in the diffuser. This means that some parts of the kinetic energy of the mixture is converted into pressure. Finally, the pressure of the emerging fluid will become slightly higher than the pressure of MED-vessels.

5.2. Contours of thermodynamic variables

In order to understand the above-mentioned processes more clearly, contours of the flow temperature and flow velocity inside the axisymmetric model of the TVC is represented in Figs. 11 and 12. As observed, these figures show a clear series of oblique shock waves immediately after the nozzle exit plane, which expands through the converging duct. These shock waves are the main source of the

Table 3
Temperature and pressure values at TVC boundaries

	Temperature, °C	Pressure
Primary flow	170	7 bar
Secondary flow	49	125 mbar
Discharge flow	69	288 mbar

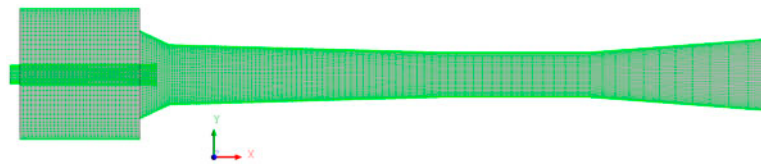


Fig. 5. Axisymmetric model of the TVC.

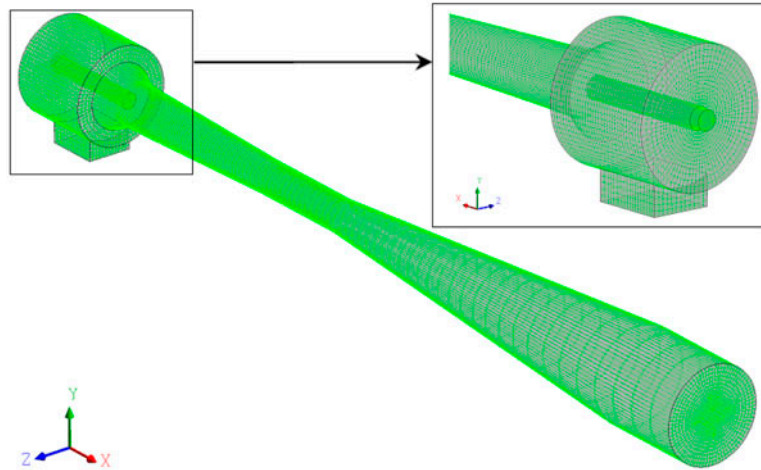


Fig. 6. Three-dimensional model of the TVC.

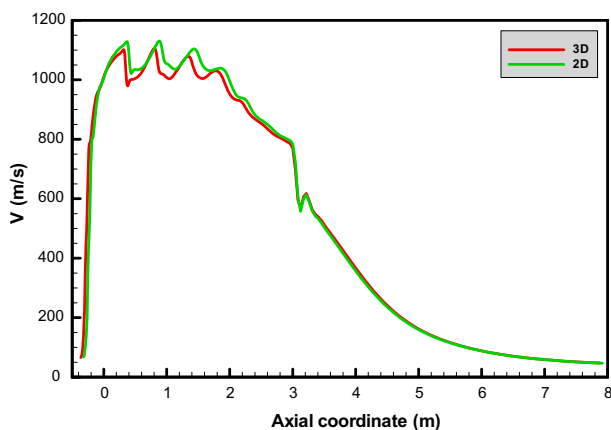


Fig. 7. Variations of the flow velocity along the main axis of the TVC.

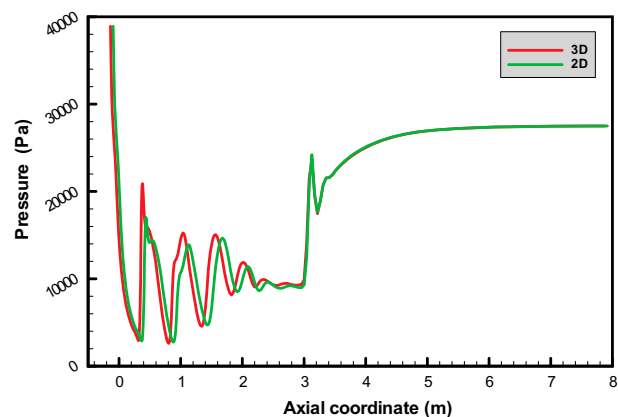


Fig. 8. Variations of the flow pressure along the main axis of the TVC.

fluctuations inside the TVC. For this reason, the overall processes inside TVCs are considered as complicated phenomena.

Another ambiguity involving the axisymmetric simulation of the TVC is the shape of inlet part that may undermine the assumption of flow symmetry inside the domain. The TVCs used in industrial

applications are usually assembled by a steam collector, which is connected to the suction chamber as shown in Fig. 6.

Hence, the shape of flow pathway should be precisely taken into account, as it may affect the overall performance of the TVC. In such situation, axisymmetric formulation is not capable of modeling the

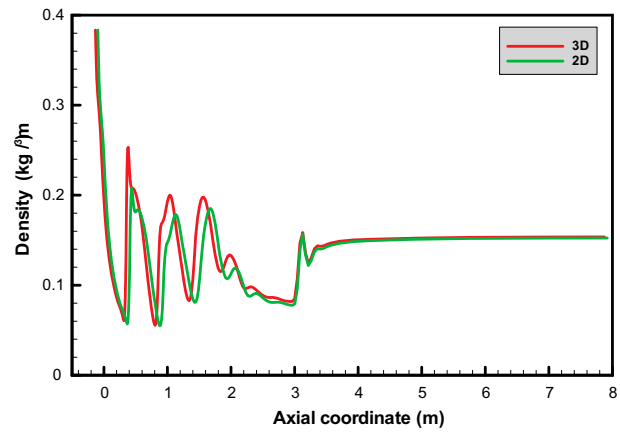
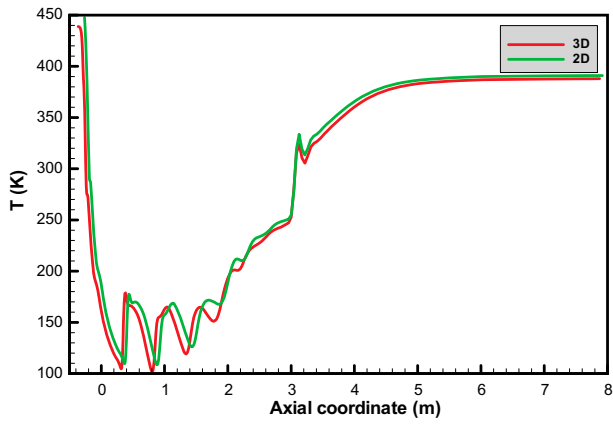


Fig. 9. Variations of the flow temperature along the main axis of the TVC.

Fig. 10. Variations of the flow density along the main axis of the TVC.

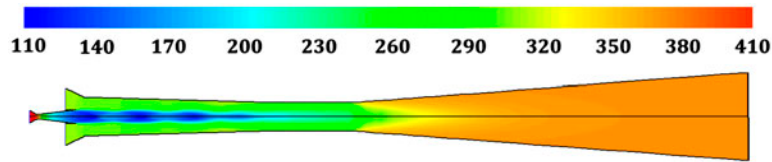


Fig. 11. Contours of the flow temperature (K) inside the axisymmetric TVC.

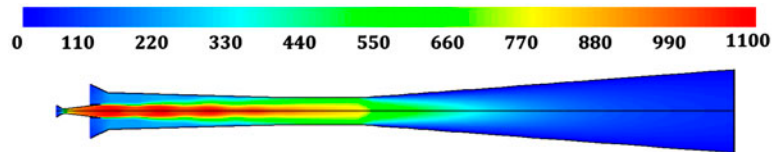


Fig. 12. Contours of the flow velocity (m/s) inside the axisymmetric TVC.

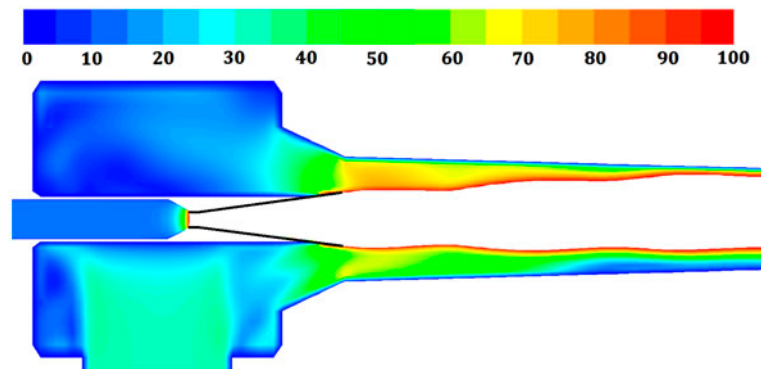


Fig. 13. Contours of the flow velocity (m/s) inside the suction chamber of the 3D TVC model.

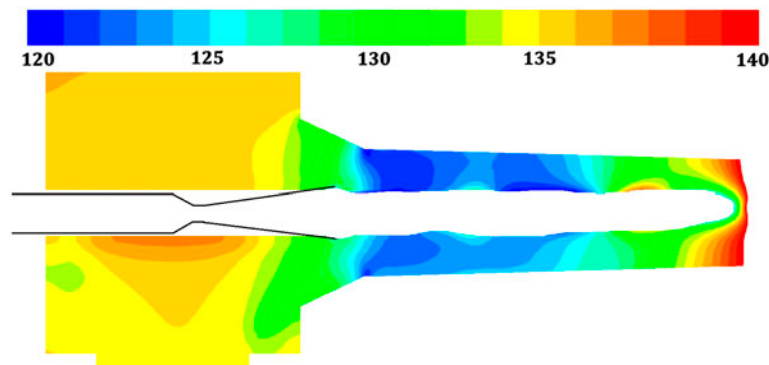


Fig. 14. Contours of the flow pressure (mbar) inside the suction chamber of the 3D TVC model.

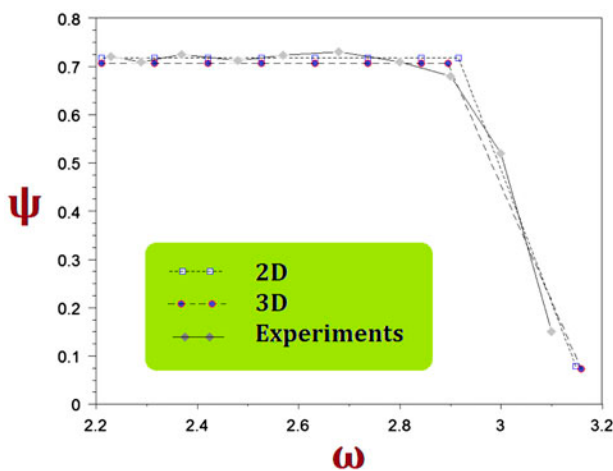


Fig. 15. Characteristic curve of the TVC based on 2D (axisymmetric) and 3D results compared with experimental data.

variations of whole flow field. Thus, it is necessary to use a full 3D simulation for the thermo-compressor.

Fig. 13 shows a limited range of variations (0–100 m/s) for displaying the contours of velocity in the non-symmetric part of the TVC. As mentioned earlier (explanations on Fig. 7), the overall range of velocity in this device is varied from 0 to 1,100 m/s. Therefore, a restricted range of variations was chosen for this picture in order to contours be illustrated in more details.

A closer look on the flow velocity on the lower and upper pathways of the inlet section reveals the existence of a small difference less than 10 m/s (~0.91%) between these two flow velocities.

The same procedure is repeated for displaying the pressure contours inside the suction chamber. As mentioned earlier (explanations on Fig. 8), the overall range of pressure in this device is varied from 0 to 8 bar (i.e. 8,000 mbar). Thus, it was preferred to plot pressure contours in the range of 120–140 mbar (i.e. available

pressure ranges in the suction chamber, before the suction stream be mixed with the motive flow), in order to contours be illustrated in more details.

As it can be seen in Fig. 14, the pressure difference in the flow of lower and upper pathways is less than 5 mbar (~0.062%). Since the upper and lower streams merge together at the end of the non-symmetric zone, the actual pressure at the inlet boundary of 2D model could be assumed nearly equal to the nominal pressure (i.e. 125 mbar).

5.3. TVC operating curve

Since the performance of the TVC is not solely depend on thermodynamic properties along the centerline, it cannot be concluded, at this time, that the axisymmetric approach is quite similar to the 3D model, unless the characteristic parameters of the TVC are extracted from both numerical models.

Fig. 15 shows the characteristic curves of two simulated models together with experimental results. As mentioned earlier, the TVC performance is expressed as a function of both entrainment ratio (ω) and compression ratio (ψ).

The trend of ω values against ψ for 3D model represents the same trend as the axisymmetric one. Furthermore, the maximum differences of ω and ψ between these two models are lower than 0.45 and 0.37%, respectively. In addition, the critical backpressure in which the ψ begins to drop is substantially better for 3D model in comparison with the experimental results.

This study is motivated by the need for a fast and simple CFD simulation method that can be used to design and evaluate the performance of a steam jet compressor. The above consequences represent the acceptable accuracy of the axisymmetric simulation in comparison with full 3D one for thermo-compressors.

Therefore, it can be judged the axisymmetric simulation is capable enough for producing acceptable flow field in the computational domain of a typical TVC, and it is commonly preferred due to lower CPU time and ease of mesh generation in 2D geometries with respect to 3D ones.

Although, the parametric study is essentially required to determine each geometrical parameter and the best condition for flow properties at boundaries, a detailed discussion on studying these parameters to design an optimized thermo-compressor is beyond the scope of current study. Such attempts may be reported in a separate technical paper focusing on the design methodology of TVC.

6. Conclusion

With the increasing intricacy of the compressible flow steam within a TVCs, it becomes necessary, not only to reveal the complicated internal phenomena, but also to introduce methods of visualization that make the flow behavior more easily interpretable. Having a non-symmetric zone in the suction pathway of a real TVC necessarily requires utilizing a three-dimensional method. However, negligible effect of this part on the overall performance of the TVC is observed.

Therefore, axisymmetric simulation is preferred as it provides reliable results inside the computational domain. It means that the simpler axisymmetric modeling of flow within a TVC is sufficient, and there is no need to use a complete three-dimensional simulation that requires more complicated grid generation and more computational cost. The results of both methods show a reasonable agreement with experimental data. Moreover, this procedure is quite capable of capturing different operational modes of the TVC at both critical and sub-critical conditions.

Acknowledgement

The authors wish to thank FanNiroo Company for its help in setting up the experimental stand and the permission to publish these valuable data.

Symbols

E	—	enthalpy
g	—	gravitational acceleration
MED	—	multi-effect desalination
p	—	pressure
Src	—	source term
t	—	time

T	—	temperature
TVC	—	thermal-vapor compressor
u	—	velocity
x	—	dummy variable
Greek		
ρ	—	density
ε	—	turbulent dissipation rate
κ	—	turbulent kinetic energy
τ	—	stress tensor
μ	—	dynamic viscosity
σ	—	liquid surface tension
ψ	—	compression ratio
ω	—	entrainment ratio

References

- [1] H.S. Aybar, Analysis of a mechanical vapor compression desalination system, *Desalination* 142 (2002) 181–186.
- [2] N.H. Aly, A.K. El-Figi, Mechanical vapor compression desalination systems – A case study, *Desalination* 158 (2003) 143–150.
- [3] I.S. Park, S.M. Park, J.S. Ha, Design and application of thermal vapor compressor for multi-effect desalination plant, *Desalination* 182 (2005) 193–202.
- [4] X. Liu, D. Liu, S. Shen, Y. Yang, F. Gao, Performance analysis of mixed feed LT-MED desalination system with thermal vapor compressor, *Desalin. Water Treat.* 42 (2012) 248–255.
- [5] N. Sharifi, M. Boroomand, An investigation of thermo-compressor design by analysis and experiment: Part 1. Validation of the numerical method, *Energy Convers. Manage.* 69 (2013) 217–227.
- [6] N. Sharifi, M. Boroomand, An investigation of thermo-compressor design by analysis and experiment: Part 2. Development of design method by using comprehensive characteristic curves, *Energy Convers. Manage.* 69 (2013) 228–237.
- [7] K. Yang, H.M. Lee, H.H. Jung, Numerical prediction of jet behavior of thermal vapor compressor, *Desalin. Water Treat.* 33 (2011) 248–254.
- [8] I.S. Park, Robust numerical analysis based design of the thermal vapor compressor shape parameters for multi-effect desalination plants, *Desalination* 242 (2009) 245–255.
- [9] S. Shen, S. Zhou, Y. Yang, L. Yang, X. Liu, Study of steam parameters on the performance of a TVC-MED desalination plant, *Desalin. Water Treat.* 33 (2011) 300–308.
- [10] R. Kouhikamali, N. Sharifi, Experience of modification of thermo-compressors in multiple effects desalination plants in Assaluyeh in Iran, *Appl. Therm. Eng.* 40 (2012) 174–180.
- [11] H.S. Choi, T.-J. Lee, Y.-G. Kim, S.-L. Song, Performance improvement of multiple-effect distiller with thermal vapor compression system by exergy analysis, *Desalination* 182 (2005) 239–249.
- [12] N. Sharifi, M. Boroomand, R. Kouhikamali, Wet steam flow energy analysis within thermo-compressors, *Energy* 47 (2012) 609–619.

- [13] R. Kouhikamali, H. Sadeghi, A. Safari, N. Sharifi, Geometrical analysis of thermo-compressors in multiple-effects distillation units based on the second law of thermodynamics, *Desalin. Water Treat.* (in press), doi: 10.1080/19443994.2013.817509.
- [14] FLUENT 6.0 User's Guide, Volume 1–5, Fluent Inc., Lebanon, NH, 2001.

Appendix A. Flowchart of CFD solver

A.1. Introducing the density based mode in FLUENT

The nonlinear governing equations were solved using the "Density-Based" method due to highly compressible flow and high level of Mach number. In the density-based solution method, the coupled system of equations (continuity, momentum, energy and species equations if available) is solved simultaneously using either the coupled explicit formulation or the coupled-implicit formulation. The manner in which the governing equations are linearized may take an implicit or explicit form with respect to the dependent variable (or set of variables) of interest [14].

In the density-based solution methods, the discrete, nonlinear governing equations are linearized to produce a system of equations for dependent variables in every computational cell. The resultant linear system is then solved to yield an updated flow field solution [14].

Because the governing equations are nonlinear (and coupled), several iterations of the solution loop must be performed before a converged solution is obtained. Each iteration consists of the steps illustrated in Fig. A.1 and outlined below:

- (1) Update the fluid properties based on the current solution. (If the calculation has just begun, the fluid properties will be updated based on the initialized solution.)
- (2) Solve the continuity, momentum, and energy equations simultaneously.
- (3) Solve equations for scalars, such as turbulence and radiation, where appropriate.
- (4) Check for convergence of the equation set.

The above steps are continued until the convergence criteria are met [14].

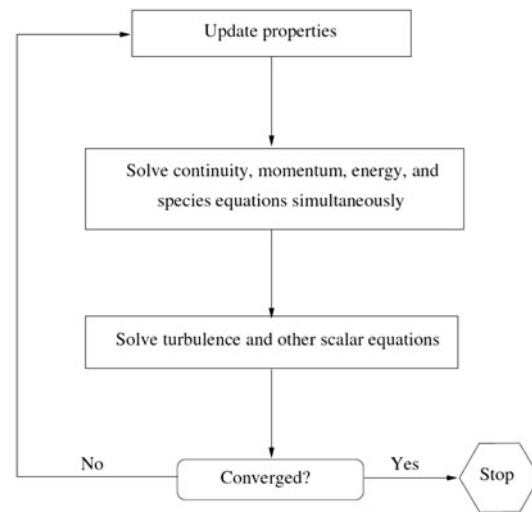


Fig. A. 1. Overview of the Density-Based method in FLUENT [14].

A.2. Inputs required for solver

The following procedures are essential for a problem to be setup correctly in FLUENT solver:

- (1) Importing a Mesh file (2D or 3D) such as those introduced in Figs. 5 and 6.
- (2) Setting the material properties adopted from FLUENT material database for water/vapor.
- (3) Setting the density of this material to be calculated based on the ideal gas model.
- (4) Setting the Boundary conditions according to Table 3.
- (5) Initializing the solver that is performed by computing from all zones (embedded in the software menus).
- (6) Setting the residuals low enough (e.g. 1e-6 or lower).
- (7) Iterating the solution until the convergence criteria are met.